Post-processing of Pixel and Object-Based Land Cover Classifications of Very High Spatial Resolution Images

Tommaso Sarzana[1], Antonino Maltese[1(✉)], Alessandra Capolupo[2], and Eufemia Tarantino[2]

[1] Università degli Studi di Palermo, 91011 Palermo, PA, Italy
antonino.maltese@unipa.it
[2] Politecnico di Bari, 70125 Bari, BA, Italy

Abstract. The state of the art is plenty of classification methods. Pixel-based methods include the most traditional ones. Although these achieved high accuracy when classifying remote sensing images, some limits emerged with the advent of very high-resolution images that enhanced the spectral heterogeneity within a class.

Therefore, in the last decade, new classification methods capable of overcoming these limits have undergone considerable development. Within this research, we compared the performances of an Object-based and a Pixel-Based classification method, the Random Forests (RF) and the Object-Based Image Analysis (OBIA), respectively. Their ability to quantify the extension and the perimeter of the elements of each class was evaluated through some performance indices. Algorithm parameters were calibrated on a subset, then, applied on the whole image. Since these algorithms perform accurately in quantifying the elements areas, but worse if we consider the perimeters length, hence, the aim of this research was to setup some post-processing techniques to improve, in particular, this latter performance.

Algorithms were applied on peculiar classes of an area comprising the *Isole dello Stagnone di Marsala* oriented natural reserve, in north-western corner of Si-cily, salt pans and agricultural settlements. The area was covered by a World View-2 multispectral image consisting of eight spectral bands spanning from visible to near-infrared wavelengths and characterized by a spatial resolution of two meters. Both classification algorithms did not quantify accurately object perimeters; especially RF. Post-processing algorithm improved the estimates, which however remained more accurate for OBIA than for RF.

Keywords: Random forest · Object-Based image analysis · Vector based generalization

1 Introduction

A large amount of studies compared Pixel-Based and Object-Based classification methods based on different image data sources [1–4] are present in literature. Aggarwal *et al.* [5] documented that the Object-Based methods allow achieving a higher accuracy

© Springer Nature Switzerland AG 2020
O. Gervasi et al. (Eds.): ICCSA 2020, LNCS 12252, pp. 797–812, 2020.
https://doi.org/10.1007/978-3-030-58811-3_57

than pixel-based methods, since these latter analyze only the spectral features while the former taking advantage also of the spatial features during the segmentation process. Recently, Cai *et al.* [6] proposed new similarity metrics to evaluate the accuracy of objects extraction from Earth Observation images in terms of area and perimeter.

Since pixel-based classification methods are based only spectral characteristics of single pixel produce erroneous small classes. Thus, post-classification algorithms were implemented to reduce the occurrence of these classes through majority focal filters [*e.g.*, 7, 8].

Object-based methods firstly groups neighboring pixels into objects through segmentation [*e.g.*, 9]. Thus, although errors always occur, they show up less frequently.

Jensen *et al*. [10] proposed a size-based filter to select and remove classes having areas smaller than a threshold.

However, classification output can be improved by applying both cleaning and smoothing post-processing algorithms. Snakes algorithms, in particular, represent a powerful tool to correct the pixelated edges derived from the classification of raster images. An overview of line smoothing algorithms in automated generalization is presented by Weibel [11]. The aim of this research was to reckon if smoothing and cleaning post-processing algorithms could be used to improve the classification accuracy in terms of area and perimeter.

2 Materials

2.1 Study Area

The *Stagnone di Marsala* is the largest coastal lagoon in Sicily (southern Italy). It is framed between 277400 and 274030 from West to East and 4187160 and 4199100 from South to North (UTM WGS84). The lagoon was declared a Regional Natural Reserve since it constitutes a peculiar ecosystem characterized by phanerogams such as Posidonia oceanica, Caulerpa prolifera and Cymodocea nodosa [*Ciraolo et al.* 12]. Isola Lunga is the largest island of the reserve. It results from the union of three small islands through salt pans. Indeed, historically the main activity practiced in the lagoon is the production of salt by evaporating the water channeled into the salt pans.

The salt collection begins in July and lasts until September/October. The raw salt is piled up in spaces called *arioni* and exposed to the first rains, which wash away the magnesium sulphate, then, the piles are covered with tiles.

The geomorphology of the coastal area is marked by a succession of marine terraces which gives the landscape a flat structure. The slope of this coastal plain in the EW direction is ≈1° going up towards an inland slightly hilly area at 100–150 m altitude.

Main cultivations are vineyards, often overlooking the sea and in any case exposed to intense sun exposure, growing on clayey sometimes rich in red soils and sandy soils. The climate is Mediterranean-insular, with hot dry summers, with sea breezes, sometimes hot African winds. The average yearly temperature is ≈18 °C, and the average annual rainfall ≈500 mm.

Cultivar characterized by white berried grapes are breed for the production of gold and amber wine, while cultivar with red berried grapes are breed for the production of ruby wine as regulated by the disciplinary of production of the Controlled Designation of Origin of the Marsala wine. The study area and the location of four representative plots are reported in Fig. 1.

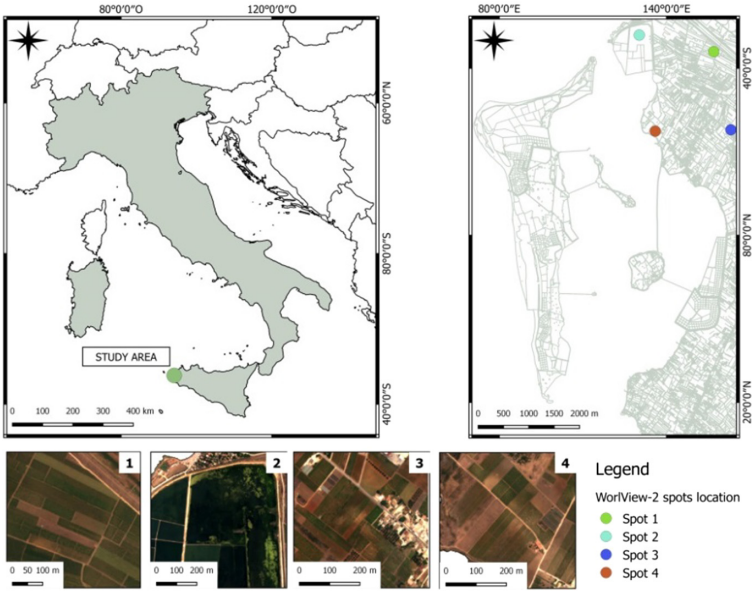

Fig. 1. Study area: location of the study area in Italy (top-left panel); map of the study area with location of the four spots (green, cyan, blue and red spots in the top right-panel) and natural color composition of the spots (lower panels). (Color figure online)

2.2 Data

Data used in this research includes satellite images and in situ spectroradiometric signatures.

Earth Observation Images. The research has been applied on a WorldView-2 (VW2) multispectral satellite image acquired on 6 August 2011 at 10/10: 30 UTC that covers a ≈58 hectares area. The multispectral image provides eight spectral bands in the visible and near infrared (NIR) parts of the spectrum: Coastal (400–450 nm), Blue: 450–510 nm, Yellow (585–625 nm), Green: 510–580 nm, Red Edge (705–745 nm), Near-IR2: 860–1040 nm, Near-IR1: 770–895 nm. The dynamic range is 11-bits per pixel.

Spectroradiometric Data. Spectroradiometric data were acquired on dark and bright natural surfaces during the satellite overpass using an ASD Field Spec Pro FR spectroradiometer covering the full solar reflected spectrum (350–2500 nm) with 10 nm spectral resolution.

3 Methodology

Smoothing and cleaning procedures were applied on classified images. Two widespread pixel-based and vector-based classification methods were chosen as representative of two different paradigms. Raster images were erstwhile calibrated in spectral reflectance at bottom of atmosphere.

3.1 Radiometric Calibration and Atmospheric Correction

The WorldView 02 (WV2) image was radiometric calibrated in reflectance and corrected by the atmospheric influence by setting up a linear relationship between spectral radiance at top of atmosphere and spectral reflectance at bottom of atmosphere, R_0 (–) according to Karpouzli and Malthus [13]. To this purpose, spectroradiometric signatures were collected in situ during the satellite acquisition over natural dark and bright targets.

3.2 Classification

Two classification techniques available on open-source SAGA GIS have been applied: an OBIA (Object-based Image Analysis) supervised and the Random Forests. For both algorithms, the applied procedure can be schematized as follows:

- Parameters setup on a subset of the study area;
- Land Use Land Cover (LULC) classification;
- Post-processing and accuracy evaluation.

During the calibration phase, parameters were assessed by computing two indices: the Areal Overall-Accuracy and the Perimeter Index-Accuracy.

To create a reference or ground truth layer a number of polygons for each class have been digitized on Google Earth. These polygons cover the whole image almost proportionally to the area of each class, following a random stratified criterion. The location of the ground truth polygons, indeed, was chosen for each class via random points generated by the *Random Points* tool of QGIS.

The ground truth polygonal layer was successively intersected with classification, allowing calculating the overall areal accuracy, AOA (%), as well as user and producer accuracies, *UA* (%) and *PA* (%), respectively (1).

$$AOA = \frac{\sum_i^n Aii}{A_{tot}} \times 100 \tag{1}$$

where, n is number of classes; A_{ii} is area of the ith class correctly classified; A_{tot} is the total area.

To assess the accuracy with which the procedure reproduces the perimeters of the objects, a perimeter accuracy index, *PAI* (%), was defined as (2):

$$PAI = \left(1 - \frac{\sum_{i=1}^{n} \left| 1 - \frac{\sum_{i=1}^{n_k} P_{obj_{i,k}}}{\sum_{i=1}^{n_k} P_{ref_{i,k}}} \right|}{n} \right) \times 100 \quad (2)$$

where, $P_{obj_{i,k}}$ is the perimeter of the ith object classified as class k; $P_{ref_{i,k}}$ is the perimeter of the ith object of the kth class in the ground truth layer.

The *PAI* was evaluated on polygons characterized by a degree of compactness less than a threshold. The compactness was evaluated via the Normalized Perimeter Index, *NPI* (−) [14]. The threshold has been chosen based on the *NPI* frequency distribution equal to 2.

$$NPI = \frac{P_{obj}}{P_{cea}} < 2 \quad (3)$$

where, P_{cea} is the perimeter of a circle with equivalent area.

Random Forest Classification. The Random Forests is among the most efficient Machine Learning pixel-based algorithms for images classification. High performances are achievable with a single calibration parameter, the *nTree* [15]. This parameter regulates the number of trees that make up the random forest. The algorithm creates a multiple decision trees by analyzing the training dataset, so that many combinations of predictive variables are explored, by maximizing the non-correlation between trees and minimizing the over-fitting [16]. After the learning phase, the most recurrent output from the trees is chosen as predicted class. The *nTree* parameter of the RF algorithm implemented in SAGA GIS was calibrated on the subset. The following orders of magnitude were tested for calibration: *nTree* = 10, 100, 1000 and 10000. In addition, the computational time and the correlation increase of the probabilities of correct prediction were also evaluated. The determination coefficient, r^2, increased with the number of tree. The calibration returned *nTree* = 1000 as the suitable value for this case study, with r^2 = 0.99%, and a computational time of one tenth of that required by 10000 trees.

OBIA Supervised Classification. The OBIA algorithm processes an image through a preliminary segmentation phase; then, classifying the segments based their spectral characteristics. A Minimum Distance method was chosen to classify the segments. The algorithm, implemented in SAGA GIS, has been calibrated by tuning the Band Width for Seed Point Generation parameter. This parameter drives the number and the size of the segments. The seeds, indeed, defines the distance within which to search for the point of minimum spectral variance [17]. The greater this distance the more heterogeneous the spectral characteristics of the segments. The following Band Width values were chosen: 2, 4, 10 and 20 m. The Band Width achieving the best performance (10 m, AOA 91.5% PAI 41%) was chosen to classify the whole study area.

3.3 Post Processing

Algorithms of cleaning and smoothing were applied to remove small classes mainly resulting from images heterogeneities and smoothing to remove the pixelated boundary of the objects resulting from the classification of the raster images.

Smoothing. An algorithm for vector smoothing has been applied to the cleaned polygon vector. The algorithm is the *Snakes* included in the module *v.generalize* of Grass. The snakes algorithm was introduced by Kass *et al*. [18] that defined the energy of a snake [19] by considering an inner and an external energy E_{I} and E_{ext} with respect to arc length s.

$$E_S = \int_0^1 (E_E + E_I) ds \tag{4}$$

The minimization of E_{S} allows obtaining a smoothed line or polygonal vector. Configuration parameters have been fixed to the default values ($\alpha = 1$, $\beta = 1$ and 1 iteration).

Cleaning. A cleaning tool from Grass *v.clean* with option *rmarea* to remove small polygonal areas and union with adjacent polygons sharing the longest arc. Configuration threshold has been set to 150 m^2 after visual inspection of the classifications.

4 Results

Confusion matrices summarizing user accuracy (UA %) and producer accuracy (PA %) for each class, and the areal overall accuracy of each classification method are reported in Tables 1 and 2 for RF and Tables 4 and 5 for OBIA.

The relative errors for each class and the average perimeter accuracy for each classification method are reported in Table 3 and 6 for RF and OBIA, respectively.

Some spots are also reported to exemplify the behavior of the classification and post-processing algorithms over each class.

4.1 Pixels Based

The following spot (Fig. 2) shows that the RF algorithm distinguishes bare soil from vegetation, while non dense and dense vegetation are difficult to distinguish.

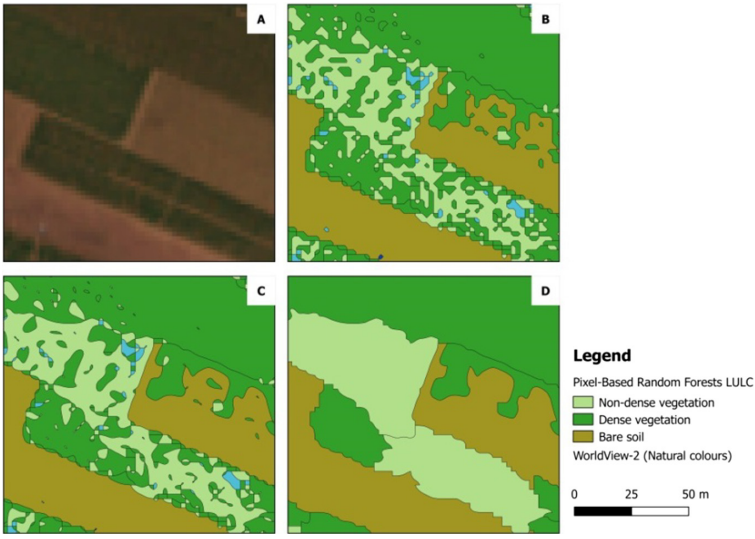

Fig. 2. Spot 1, vegetated and bare soils: A) WV2 Natural colours composition; B) RF LULC; C) after smoothing; D) after cleaning

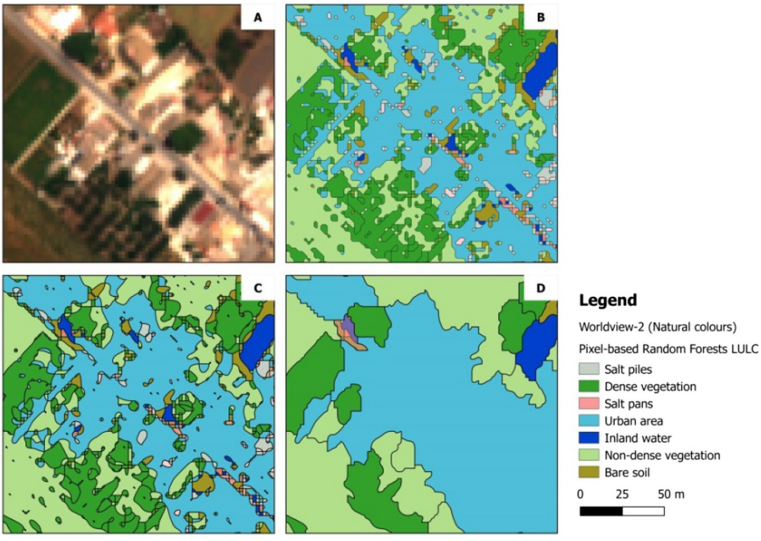

Fig. 3. Spot 2, urban area: A) WV2 Natural colours composition; B) RF LULC; C) after smoothing; D) after cleaning.

In Fig. 3 are clearly evident some classification errors, indeed urban and salt classes are confused. Omissions and commissions errors are partly reduced by applying the cleaning algorithm.

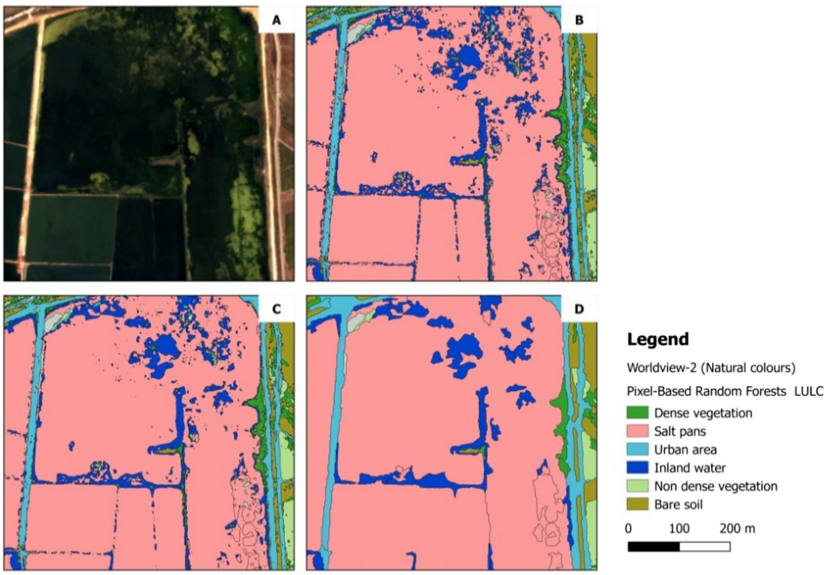

Fig. 4. Spot 3, salt pans: A) WV2 Natural colours composition; B) RF LULC; C) after smoothing; D) after cleaning.

The last spot (Fig. 4) exemplifies the behaviour of the RF classifier over salt pans. The need to remove polygons with small areas is evident. This need diminishes in OBIA classification (Fig. 7).

Table 1. RF confusion matrix with User Accuracy (*UA* %), Producer Accuracy (*PA* %) and Area overall accuracy (*AOA* %)

Ground truth → Classification ↓	Acronym	NDV	DV	BS	SPa	SPi	IW	UA	***PA***
Non-dense vegetation	NDV	7.7	1.2	0.5				0.1	**81.1**
Dense vegetation	DV	2.4	15.5	2.1			0.1		**77.1**
Bare soil	BS	0.5	2.0	11.8			0.2		**81.4**
Salt pans	SPa				33.8	0.1	3.3	0.4	**89.9**
Salt piles	SPi				0.1	5.2	0.1	1.6	**74.3**
Inland water	IW		0.8	0.1	0.3		4.3		**78.2**
Urban area	UA	0.6	0.4	1.1		0.1	0.2	3.3	**57.9**
	UA	**68.8**	**77.9**	**75.6**	**98.8**	**96.3**	**52.4**	**61.1**	**OA 81.7**

Summarizing, the lowest *PA* was 57.9% for urban areas; while, the lowest *UA* was 52.4% for inland water whose ground truths are often are classified salt piles. Overall, the *AOA* was 81.7%.

Table 2. RF confusion matrix after post processing with User accuracy *UA* (%), Producer accuracy *PA* (%), Areal Overall Accuracy *AOA* (%).

Ground truth → Classification ↓	Acronym	NDV	DV	BS	SPa	SPi	IW	UA	***PA***
Non-dense vegetation	NDV	8.1	0.6	0.4					**89.0**
Dense vegetation	DV	1.9	15.5	1.5					**82.0**
Bare soil	BS	0.4	2.1	13.0					**83.9**
Salt pans	SPa				35.1		3.2	0.2	**91.2**
Salt piles	SPi				0.1	5.1	0.1	1.4	**76.1**
Inland water	IW		0.8		0.1		4.5		**83.3**
Urban area	UA	0.4	0.5	1.0	0.0	0.1	0.1	3.7	**63.8**
	UA	**75.0**	**79.5**	**81.8**	**99.4**	**98.1**	**57.0**	**69.8**	***AOA*** **85.1**

After post-processing, the *PA* for urban areas increased to 63.8%; while, the *UA* for inland water increased to 57.0% for whose ground truths are still often classified salt piles. Overall, the *AOA* increased to 85.1%. The analysis of the probability of random agreement evaluated according to the Cohen's kappa resulted in *K* equal to 0.77 after the RF classification, then, it raised to 0.81 after the post processing.

Table 3. RF relative errors $\boldsymbol{\rho_E}$ (%) of class perimeters with NPI < 2 and after post-processing

Class	Acronym	Classification ρ_E	Post-processing ρ_E
Non-dense vegetation	NDV	14	17
Dense vegetation	DV	22	19
Bare soil	BS	27	28
Salt pans	Spa	133	137
Salt piles	SPi	42	29
Inland water	IW	33	34
Urban area	UA	80	56
Perimeter accuracy index:		49.5	54.3

The accuracy in classifying the object perimeters was very low (49.51% on the average). The relative error decreased significantly after post-processing for salt piles and for urban areas (−13% and −24%, respectively). Accuracy achieved remains quite low since classification algorithms are not able to distinguish two objects belonging to the same class when the splitting element has a thickness lower that the spatial resolution of the images (for instance, two contiguous salt pans not identified as different objects since their boundary wall was smaller than half a meter).

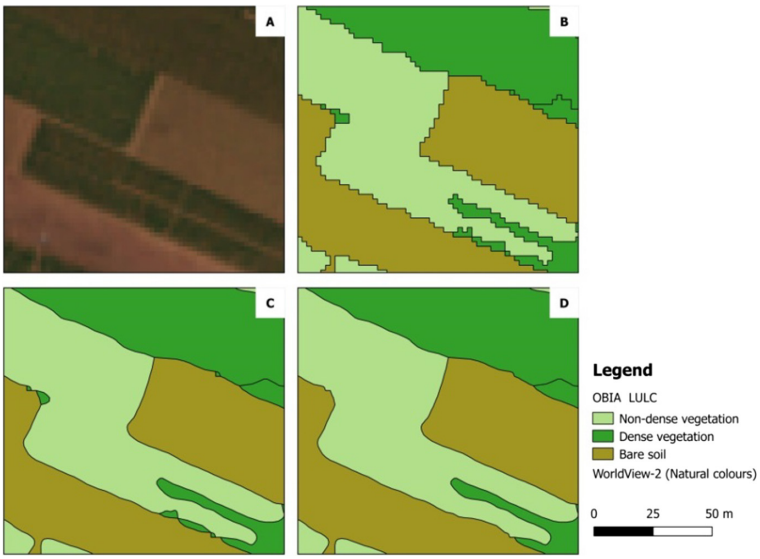

Fig. 5. Spot 1, vegetated and bare soils: A) WV2 Natural colours composition; B) OBIA LULC; C) after smoothing; D) after cleaning.

4.2 Object Based

The following spots exemplify omission and commission errors between vegetated and bare soil (Fig. 5) and among urban area, salt piles and bare soil (Fig. 6). These errors are reduced by applying the cleaning algorithm.

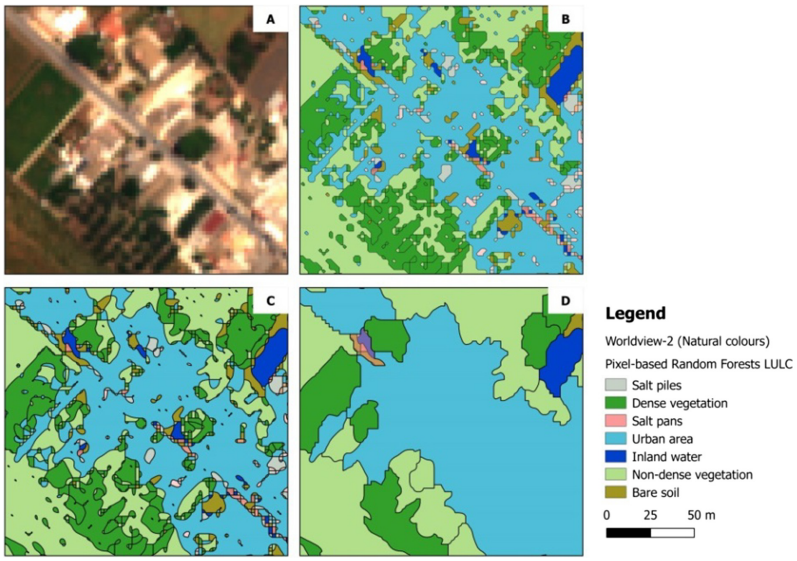

Fig. 6. Spot 2, urban area: A) WV2 Natural colours composition; B) OBIA LULC; C) after smoothing; D) after cleaning.

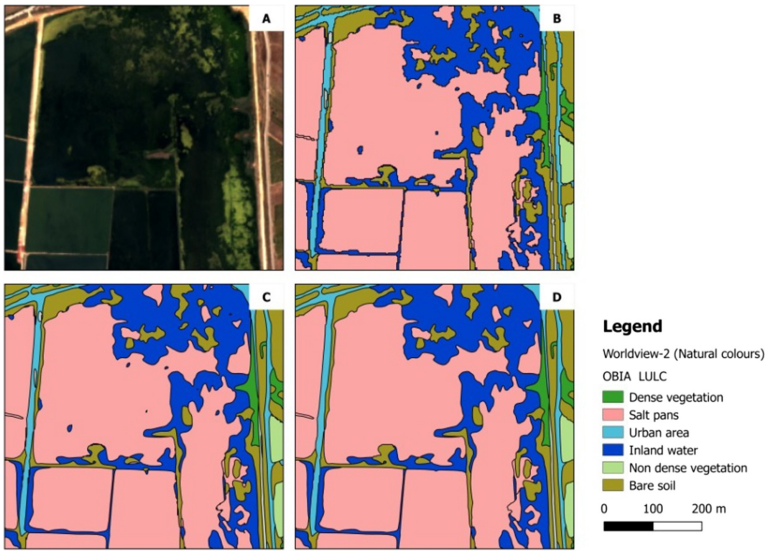

Fig. 7. Spot 3, salt pans: A) WV2 CIR composition; B) OBIA LULC; C) after smoothing, D) after cleaning.

The spot in Fig. 7 exemplifies the effects of post processing on salt pans. Differently than in RF classification, the segmentation in OBIA, incorporates in homogeneous areas adjacent pixels with some heterogeneity, thus reducing the need of post processing.

Table 4. OBIA confusion matrix with User accuracy *UA* (%), Producer accuracy *PA* (%), Areal Overall Accuracy *AOA (%)*.

Ground truth → Classification ↓	Acronym	AP	DV	BS	SPa	SPi	IW	UA	***PA***
Non-dense vegetation	AP	4.0	0.8	0.1				0.9	**69.0**
Dense vegetation	DV	1.5	5.2	1.3				0.1	**64.2**
Bare soil	BS	0.3	1.4	24.3	0.2		0.2	0.7	**89.7**
Salt pans	SPa				38.8	0.5	0.6		**97.2**
Salt piles	SPi			0.2	2.1	3.1		2.5	**39.2**
Inland water	IW				0.9		3.8		**80.9**
Urban area	UA		0.1	0.6	0.2		0.1	5.7	**85.1**
	UA	**69.0**	**69.8**	**91.7**	**91.9**	**86.1**	**80.9**	**57.6**	***AOA*** **84.7**

Summarizing, the lowest *PA* was 39.2% for salt piles a class, that often corresponds to salt pans and urban areas ground truths; while, the lowest *UA* was 57.6% for urban areas whose ground truths are often are classified salt piles. Overall, the *AOA* was 84.7%.

Table 5. OBIA confusion matrix after post processing with *UA* (%), *PA* (%) *AOA* (%)

Ground truth → Classification ↓	Acronym	NDV	DV	BS	SPa	SPi	IW	UA	***PA***
Non-dense vegetation	NDV	4.1	1.0	0.1				0.9	**67.4**
Dense vegetation	DV	1.5	5.3	1.3				0.1	**64.8**
Bare soil	BS	0.3	1.4	24.8	0.2		0.3	0.6	**89.8**
Salt pans	SPa				39.5	0.4	0.6		**97.4**
Salt piles	SPi			0.2	0.7	3.1		2.5	**47.8**
Inland water	IW				0.9		3.8		**80.6**
Urban area	UA			0.6	0.1			5.7	**87.1**
	UA	**69.5**	**68.8**	**91.9**	**95.4**	**88.6**	**80.9**	**58.2**	***AOA*** **86.3**

After the post-processing, the *PA* for salt piles increased to 47,8%, this class often corresponds to urban areas ground truths; while, the *UA* for urban areas increased to 58.2% with the urban area ground truth still sometimes classified as salt piles. Overall, the *AOA* slightly increased to 86.3% (+1.6%).

The expected agreement due to the case resulted in $K = 0.79$ after the OBIA classification, that increased to 0.81 after the post processing.

Table 6. OBIA $\boldsymbol{\rho_E}$ (%) of class perimeters with NPI < 2 and after post-processing

Class	Acronym	Classification $\boldsymbol{\rho_E}$	Post-processing $\boldsymbol{\rho_E}$
Non-dense vegetation	NDV	36	36
Dense vegetation	DV	39	38
Bare soil	BS	37	37
Salt pans	Spa	25	22
Salt piles	SPi	32	31
Inland water	IW	20	20
Urban area	UA	32	32
Perimeter accuracy index:		68.4	69.1

The accuracy in classifying the object perimeters was quite low (68.1% on the average). The relative error decreased slightly after post-processing (0–3%).

Accuracy in distinguish two objects belonging to a class when separated by an object having thickness lower 2 m (images spatial resolution) is enhanced by splitting the two objects during the segmentation phase. For instance, ρ_E was $\sim$130% for salt

pans after RF classification (Table 3), while for the same class OBIA reached a $\rho_E \cong$ 25% (Table 6).

4.3 Comparison

The spot in Fig. 8 shows a comparison between OBIA and RF classification (panels B and C, respectively). It is clear that OBIA is more efficient in reducing classification errors due to spectral heterogeneity. Thus, post processing is more effective on RF (panel D) that in OBIA (panel E).

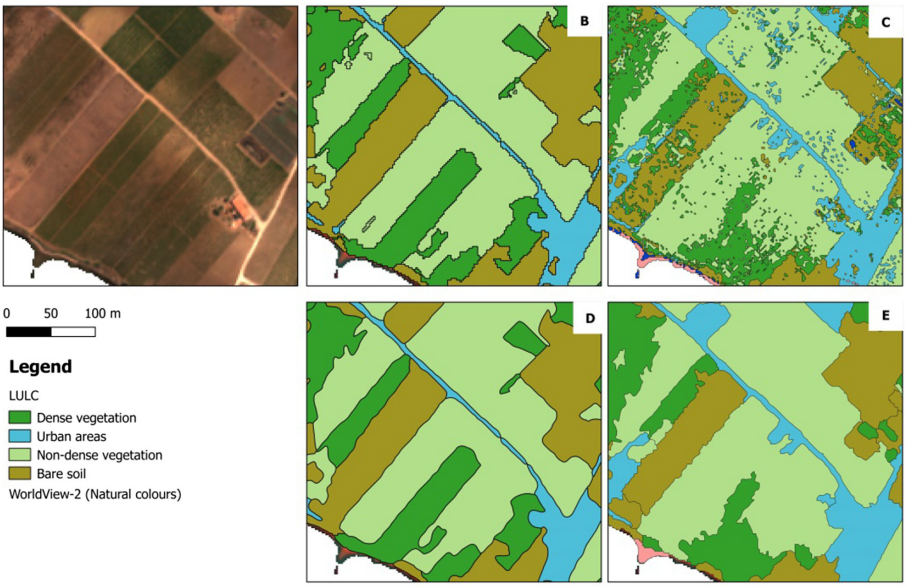

Fig. 8. Spot 4, OBIA vs. RF comparison: A) WV-2 Natural colours; B) Random Forests LULC; D) Post-processed OBIA LULC; E) Post-processed Random Forests LULC.

The comparison between the two classification methods shows that both of the classification methods accurately identified the classes and the object areas: the *AOA* were ≈81% and ≈85% for RF and OBIA, respectively (Table 7). However, RF requires a post-processing to reach accuracies comparable to that OBIA. Indeed, after post-processing, the *AOA* increased significantly for RF (up to ≈85%) while slightly increases for OBIA (≈86%). Objects perimeters were assessed with much lower accuracy. It was even lower that 50% for RF, while it was lower than 70% for OBIA. The OBIA algorithm, indeed takes is able to merge adjacent heterogeneous pixels to those characterizing a class during the segmentation process. Although the perimeter accuracy it increased significantly for RF (up to ≈55%) it remains lower than for OBIA. Differences are probably due to the classification units the pixel for the RF and

the segment for the OBIA. Indeed, heterogeneity within pixels belonging to a class is higher than that of segments belonging to the same class, thus, increasing the need for a post processing of pixel-based classifications.

Table 7. RF vs. OBIA overall areal accuracy and perimeter accuracy indexes

Indexes	RF	RF post-processing	OBIA	OBIA post-processing
Area overall accuracy	81.5	85	84.7	86.3
Perimeter accuracy	49.5	54.3	68.4	69.1

5 Conclusions

The aim of this paper was to explore the post-processing techniques to improve areal and perimeter accuracy of a pixel-based and an object-based algorithm.

Classification algorithms implemented in SAGA GIS were calibrated on a subset and then applied over the whole study area. Post-processing algorithms implemented in GIS were applied then to improve the classification.

The OBIA vector based and the Random Forests pixel based algorithms were tested on a WorldView-2 multispectral image acquired at 2 m spatial resolution.

Algorithms were applied on an area comprising the Isole dello Stagnone di Marsala oriented natural reserve, in north-western corner of Sicily. In particular, algorithms were tested on Isola Lunga island in the lagoon and on the agricultural area settled in the eastern coast of the lagoon.

The algorithms parameters calibration were carried out by quantifying the areal overall accuracy and a perimeter accuracy index.

Both algorithms reached an areal overall accuracy higher than $\sim 80\%$; however, much lower performances characterized the algorithms in the quantification of the object perimeters: the perimeter index was $\sim 50\%$ for Random Forests and less than 70% for OBIA. Then, to enhance accuracies, two post-processing steps were developed: a smoothing algorithm (the Snakes algorithm implemented in *v.generalize*) to smooth pixelated polygons resulting from a raster classification; and a cleaning algorithm (*v.clean* with *rmarea* option) to remove small classes (<150 m^2) resulting from images spectral heterogeneities. The accuracy in reproducing objects perimeters increased significantly for RF (+5%) but even so remained lower than that OBIA.

We are planning to apply a machine learning classification method, such as a Random Forests, to an object-based segmentation, thus coupling the learning ability of the radiometric characteristics typical of machine learning and the minimization of the radiometric heterogeneity typical of an object based segmentation.

With the increasing availability of multispectral and hyperspectral images, as the number of spectral bands increases an analysis of spectral separability becomes progressively more necessary to assess the contribution of each band of the spectral separability.

Acknowledgments. The authors would like to thank G. Ciraolo for helping in collecting spectroradiometric data and for his technical advices.

References

1. Liu, D., Xia, F.: Assessing object-based classification: advantages and limitations. Rem. Sens. Lett. **1**(4), 187–194 (2010)
2. Tarantino, E., Figorito, B.: Mapping rural areas with widespread plastic covered vineyards using true color aerial data. Rem. Sens. **4**(7), 1913–1928 (2012)
3. Koc-San, D.: Evaluation of different classification techniques for the detection of glass and plastic greenhouses from WorldView-2 satellite imagery. J. Appl. Rem. Sens. **7**(1), 073553 (2013)
4. Tehrany, M.S., Pradhan, B., Jebuv, M.N.: A comparative assessment between object and pixel-based classification approaches for land use/land cover mapping using SPOT 5 imagery. Geocarto Int. **29**(4), 351–369 (2014)
5. Aggarwal, N., Srivastava, M., Dutta, M.: Comparative analysis of pixel-based and object-based classification of high resolution remote sensing images – a review. Int. J. Eng. Trends Technol. (IJETT) **38**(1), 5–11 (2016)
6. Cai, L., Shi, W., Miao, Z., Hao, M.: Accuracy assessment measures for object extraction from remote sensing images. Rem. Sens **10**(2), 303 (2108)
7. Tomas, I.L.: Spatial postprocessing of spectrally classified Landsat data. Photogram. Eng. Rem. Sens. **46**, 1201–1206 (1980)
8. Townshend, J.R.G.: The enhancement of computer classification by logical smoothing. Photogram. Eng. Rem. Sens. **52**, 213–221 (1986)
9. Benz, U.C., Hofmann, P., Willhauck, G., Lingenfelder, I., Heynen, M.: Multi-resolution, object-oriented fuzzy analysis of remote sensing data for GIS-ready information. ISPRS J. Photogram. Rem. Sens. **58**, 239–258 (2004)
10. Jensen, J.R., Qiu, F., Patterson, K.: A neural network image interpretation system to extract rural and urban land use and land cover information from remote sensor data. Geocarto Int. **16**(1), 1–10 (2001)
11. Weibel, R.: Generalization of spatial data: principles and selected algorithms. In: van Kreveld, M., Nievergelt, J., Roos, T., Widmayer, P. (eds.) CISM School 1996. LNCS, vol. 1340, pp. 99–152. Springer, Heidelberg (1997). https://doi.org/10.1007/3-540-63818-0_5
12. Ciraolo, G., Cox, E., La Loggia, G., Maltese, A.: The classification of submerged vegetation using hyperspectral MIVIS data. Ann. Geophys. **49**(1), 287–294 (2006)
13. Karpouzli, E., Malthus, T.: The empirical line method for the atmospheric correction of IKONOS imagery. Int. J. Rem. Sens. **24**, 1143–1150 (2003)
14. Pipitone, C., Maltese, A., Dardanelli, G., Capodici, F., Lo Brutto, M., La Loggia, G.: Detection of a reservoir water level using shape similarity metrics. In: Remote Sensing for Agriculture, Ecosystems, and Hydrology XIX, Proceedings, vol. 10421, p. 104211L (2017)
15. Duro, D., Franklin, E., Dubé, G.: A comparison of pixel-based and object-based image analysis with selected machine learning algorithms for the classification of agricultural landscapes using SPOT-5 HRG imagery. Rem. Sens. Environ. **1**(18), 259–272 (2012)
16. Breiman, L.: Random Forests. Mach. Learn. **45**, 5–32 (2001)
17. Böhner, J., Selige, T., Ringeler, A.: Image segmentation using representativeness analysis and region growing. Göttinger. Geogr. Abh. **115**, 29–38 (2006)

18. Kass, M., Witkin, A., Terzopoulos, D.: Snakes: active contour models. In: Proceedings of the First International Conference on Computer Vision, pp. 259–268. IEEE Computer Society Press (1987)
19. Burghardt, D.: Glättung mit Snakes. Festschrift zum 65. Geburtstag von Prof. Dr. Ing. habil. Siegfried Meier. TU Dresden (2002)